

Accepted Manuscript

Effects of ply clustering in laminated composite plates under low-velocity impact loading

E.V. González, P. Maimí, P.P. Camanho, C.S. Lopes, N. Blanco

PII: S0266-3538(10)00486-0
DOI: [10.1016/j.compscitech.2010.12.018](https://doi.org/10.1016/j.compscitech.2010.12.018)
Reference: CSTE 4883

To appear in: *Composites Science and Technology*

Received Date: 15 July 2010
Revised Date: 6 December 2010
Accepted Date: 12 December 2010

Please cite this article as: González, E.V., Maimí, P., Camanho, P.P., Lopes, C.S., Blanco, N., Effects of ply clustering in laminated composite plates under low-velocity impact loading, *Composites Science and Technology* (2010), doi: [10.1016/j.compscitech.2010.12.018](https://doi.org/10.1016/j.compscitech.2010.12.018)

This is a PDF file of an unedited manuscript that has been accepted for publication. As a service to our customers we are providing this early version of the manuscript. The manuscript will undergo copyediting, typesetting, and review of the resulting proof before it is published in its final form. Please note that during the production process errors may be discovered which could affect the content, and all legal disclaimers that apply to the journal pertain.



Effects of ply clustering in laminated composite plates under low-velocity impact loading

E.V. González^a, P. Maimí^a, P.P. Camanho^{b,*}, C.S. Lopes^c, N. Blanco^a

^aAMADE, Polytechnic School, University of Girona, Campus Montilivi s/n, 17071 Girona, Spain

^bDEMec, Faculdade de Engenharia, Universidade do Porto, Rua Dr. Roberto Frias, 4200-465, Porto, Portugal

^cINEGI-Institute of Mechanical Engineering and Industrial Management, Universidade do Porto, Rua Dr. Roberto Frias, 4200-465, Porto, Portugal

Abstract

This paper presents a study of the effects of ply clustering on polymer-based laminated composite plates subjected to a drop-weight impact loading. The tools used to define the impact configurations, as well as the experimental results obtained, are described in detail. These tools are simplified analytical models for the description of the impact behavior and of the damage thresholds that result in a significant reduction on the structure stiffness and strength, caused by delamination. The results obtained demonstrate that the analytical tools are useful to define the impact configurations, to obtain a preliminary understanding of the effects of each parameter that can influence the response, and to interpret the experimental results. It is concluded that ply clustering reduces the damage resistance of the structure. However, the damage tolerance assessed by the compression after impact tests is unaffected by ply clustering.

Keywords: A. Polymer-matrix composite, A. Laminates, B. Impact behavior, B. Delamination, C. Damage tolerance.

*Corresponding author

Email address: pcamanho@fe.up.pt (P.P. Camanho)

1. Introduction

The prediction of damage in polymer-based laminated composite structures induced by the impact of an external object is a complex task. Damage results from the interaction between different failure mechanisms (matrix cracking, fiber-matrix interface debonding, delamination, and fiber breakage) and depends on the governing parameters of the impact event. These parameters can be grouped in three sets: structural parameters (shape, thickness, size, lamina type, material properties, density, stacking sequence, and boundary conditions), impactor parameters (shape, size, material properties, mass, velocity, and incidence angle), and the environmental conditions. The identification of the initiation and the propagation of the damage modes is quite relevant because it yields information regarding the residual strength of the structure [1].

Experimental evidence shows that impact damage is directly related to the nature of the impact behavior which, in turn, is controlled by the governing parameters. Therefore, it is useful to know the effects of each parameter on the impact behavior, and thus to have a qualitative understanding of the possible damage mechanisms that can occur. For example, under constant energy impact conditions, a quasi-static type of impact behavior will result mostly in delamination damage, whereas in a dilatational wave-controlled type of impact behavior will result mostly in permanent indentation and fiber breakage at the impact site. There are approaches in the literature, based on simplified analytical models, which predict the type of the impact response for a determined configuration, such as impact on flat and rectangular laminated composite plates [2, 3]. The initial knowledge of the impact behavior not only helps in assessing the possible type of damage induced, but it is also useful for selecting a proper simplified analytical model to describe the impact event, for the development of efficient numerical models, and for planning test programs.

The analytical models give fast predictive results for a given impact configuration. Generally, these analytical models are limited to simple geometries of the structure and are

defined by nonlinear differential equations or integral equations which describe the response of the system until damage onset [4, 5], i.e., in the elastic regime. To bridge the analytical elastic prediction of the impact and the onset of damage, the maximum elastic impact force is typically used, and it is compared with a damage threshold allowable. Damage occurs if the predicted elastic impact force is greater than an appropriate threshold for the corresponding dynamic response type [6–10]. Therefore, the impact force is a key parameter in determining the criticality of an impact, i.e., the risk for initiating damage.

Accordingly, the analytical models can be used to compare different impact cases enabling the study of a selected parameter that can influence the response, such as the effect of the ply clustering, i.e., the effect of ply thickness.

Many works available in the literature deal with the effects of ply clustering on laminated composite structures with different geometries and loading conditions. Wisnom et al. [11] showed that ply clustering reduces the tensile strength of un-notched quasi-isotropic laminates type $[(45_m/90_m/-45_m/0_m)]_{nS}$, and the failure was clearly affected by delaminations initiated from the free edge. Tensile experiments on same type laminates with a centrally located open hole, performed by Green et al. [12], showed that specimens with dispersed single plies failed by fiber fracture. However, specimens with the same overall thickness but composed of groups of four clustered plies failed by delamination, with a trend showing an increasing strength with increasing hole sizes. These results were further analyzed by Wisnom et al. [13, 14], where the compressive loading case was also included [14]. Viot et al. [15] studied the scaling effect of increasing the ply clustering and the in-plane sizes of rectangular cross-ply laminates subjected to low-velocity impact loading. However, the effect of just ply clustering was not clearly highlighted since the responses were also affected by the scaling of the in-plane sizes.

The transverse tensile and shear strengths of a ply are function of the ply thickness, of the ply position in the laminate, and of the fiber orientation of the adjacent plies. This

is called the in-situ effect [16, 17]. Thick plies present less resistance to matrix cracking. In addition, matrix cracks often act as initiation points for delaminations which, in turn, are easier to propagate when thick plies are present [18].

Fuoss et al. [19] found that ply clustering reduces the damage resistance of a laminate when it is loaded by low-velocity impact, resulting in an increased delamination area. Stacking plies with the same fiber orientation increases the interlaminar shear stresses at the adjacent interfaces due to the increased difference in the bending stiffness of the ply groups. This increase in stress, in turn, leads to larger delaminations. Ply clustering also reduces the number of interfaces available for delamination, because delamination typically occurs at interfaces with different fiber orientations. Reducing the number of locations available for delamination will increase the delamination size at the remaining interfaces [20, 21], since delamination acts as an energy dissipating mechanism during the impact event.

The effect of clustering on the damage tolerance, assessed by means of the residual compressive strength, is not yet fully clear. In fact, the compressive strength decreases if the plate bending stiffness is reduced. In addition, the laminate bending stiffness decreases if the size of the delaminations created by impact is large (i.e. when clustering is increased) but also when the number of delamination planes is increased (i.e. when clustering is reduced). Therefore, given these counteracting effects, it is difficult to assess the effect of ply clustering on the damage tolerance of a structure.

The aim of this paper is to study the ply clustering effect on rectangular, flat and monolithic laminated composite plates subjected to a drop-weight impact of an hemispherical impactor. In order to carry out this study, the procedure selected to define the impact tests, as well as the experimental results obtained, are described in detail. The procedure for the design of the experiments is of great importance since it must ensure that one given analysis is focused on the effects of only one parameter. Moreover, the

procedure must provide a qualitative understanding whether damage will occur, as well as its type and extension. The procedure used here is mainly based on the impact characterization diagram proposed by Christoforou and Yigit [2, 7, 22, 23]. Given an impact configuration, the diagram predicts the behavior type and the maximum impact force by calculating only two key dimensionless parameters.

Accordingly, the content of this paper is structured as follows. Firstly, the impact characterization diagram developed by Christoforou and Yigit, and related analytical impact models are explained. Secondly, the analytical damage thresholds for delamination available in the literature are described. Based on the analytical impact models and on the damage thresholds, the definition of the impact configurations for the ply clustering study assuring the damage occurrence is presented. Then, the experimental results of the configurations considered are shown and discussed in detail, showing the effect of the ply clustering on the damage resistance and on the damage tolerance. The experimental results comprise the data from the impact tests, Non-Destructive Inspections (NDI) and Compression After Impact (CAI) tests. Finally, in order to check the accuracy and the suitability of the analytical tools, comparisons between the experimental results and the analytical predictions are presented.

2. Analytical impact modeling

2.1. Impact behaviors

Before describing the impact characterization diagram developed by Christoforou and Yigit [2, 7, 22, 23], and related analytical impact models, it is useful to review the different types of impact responses for plates (i.e. impact behaviors), as the response type is crucial to have a qualitative insight of the resulting possible damage, and for the selection of analytical simplified models and well-suited damage thresholds. Detailed descriptions of the impact behaviors are given by Olsson [3–6, 24, 25], by Christoforou and Yigit

[2, 7, 22, 23], by Abrate [8, 26], and by Lin and Fatt [27].

According to Olsson [4], three extreme plate behaviors can be encountered in an impact event, those are represented in Fig. 1. Fig. 1.a shows an impact response at which the contact time is close to the time required to propagate the compressive stress waves in the through-the-thickness direction. This behavior is typically associated with ballistic impact, and often causes localized and easily detectable damage. The response depicted in Fig. 1.b corresponds to the case where the impact time is longer than the time needed by the compressive waves to travel in the through-the-thickness direction, but not enough so the dispersive flexural and shear waves reach the plate boundaries. Therefore, the response is governed by the flexural and shear waves, and typically occurs in high-velocity impacts of small mass projectiles. Finally, the response shown in Fig. 1.c corresponds to impacts with contact times that allow the flexural and shear waves to be reflected many times from the impact point to the plate boundaries and vice versa, so the resulting deflection and impact load approach to a purely static loading case. In this case, the response is influenced by the in-plane plate size and the boundary conditions.

Typically, the responses of Figs. 1.b and 1.c yield to the so-called Barely Visible Impact Damage (BVID), so NDI methods should be applied to detect the hidden damage.

[Figure 1 about here.]

The impact behaviors described are often referenced in the literature as: (a) three-dimensional wave-controlled, through-the-thickness wave-controlled, or ballistic impact; (b) global behavior with no size effects, flexural and shear wave-controlled, or impact on an infinite plate; (c) fully-global or quasi-static impact behavior. If the global response of the plate can be neglected (extreme case of (b)), this behavior is typically called half-space impact.

2.2. Impact characterization diagram

The impact characterization diagram proposed by Christoforou and Yigit [2, 7, 22, 23] predicts the behavior type, as well as the maximum elastic impact force for a wide range of impact cases. The construction of the diagram is based on simplified analytical models of the infinite plate and the quasi-static impact behaviors. Ballistic behavior is beyond the scope of the characterization diagram.

The analytical models describe the motion of the impactor, the motion of the structure, and the local deflections in the area surrounding the impact point. The motion of the impactor w_i is defined as the sum of the local deflections due to the indentation α and the displacement of the mid-plane of the plate w_o at the impact point, $w_i = \alpha + w_o$. The inertial load of the impactor $F_i = -M_i\ddot{w}_i$ (where M_i is the impactor mass) is equal to the contact load, F_c , and to the load due to plate deflection, F_o , i.e., $F_i = F_c = F_o$.

To consider the local deflections, a contact law is commonly used and relates the contact load and the indentation as:

$$F_c = k_\alpha \alpha^q \quad (1)$$

where k_α is the contact stiffness and q is a power parameter. The diagram uses a linearized contact law of the elastic-plastic contact model proposed by Yigit and Christoforou [28] that results in closed-form solutions for the simplified models. Accordingly, the power q is equal to one and the contact stiffness is defined as $k_\alpha = 5.2RY_C$ [2], where R is the impactor tip radius and Y_C is the compressive strength of the laminate.

The definition of the load due to the plate deflections F_o when dilatational waves are not important is given by the so-called complete analytical models [2, 26]. These models use the governing equations of a laminated composite plate resulting from a selected plate theory, a linear constitutive law, and the corresponding boundary and initial conditions.

The displacement solution w_o for simply supported plates is obtained by the Navier method [29], which assumes that w_o can be expressed as a double trigonometric series. The problem can be integrated in the time by means of a numerical procedure, such as the Newmark integration method [30].

The definition of the load due to the plate deflections for the extreme behaviors, infinite plate and quasi-static, can be deduced by means of the complete analytical model. Based on the work of Zener [31] and Olsson [3, 32], the deflection load for infinite plate behavior is approached to $F_o = 8\sqrt{I_1 D^*} \dot{w}_o$ if shear effects are neglected, where the inertial term I_1 is the plate mass M_p divided by the in-plane area. The term D^* is called effective plate stiffness which is defined by fairly complicated expressions involving elliptic functions. Knowing that D_{ij} are the bending constitutive components of the plate, a sufficient approximation of D^* is [3, 6]:

$$D^* \approx \sqrt{\left(\frac{A+1}{2}\right) D_{11} D_{22}}, \quad \text{where } A = \frac{D_{12} + 2D_{66}}{\sqrt{D_{11} D_{22}}} \quad (2)$$

The deflection generated in an impact with quasi-static behavior is similar to the static response. By adding the non-linear membrane effect, which is not considered in the formulation of the complete analytical model, the deflection load can be approached as $F_o = k_{bs} w_o + k_m w_o^3 + M_p^* \ddot{w}_o$ [33]. The terms M_p^* , k_{bs} and k_m are respectively the equivalent lumped mass of the structure, and the bending-shearing and the membrane stiffnesses of the plate. These terms are function of the boundary conditions, and of the shape and configuration of the laminate. For a simply supported rectangular plate, the equivalent mass is approached as $M_p^* = M_p/4$. The stiffnesses k_{bs} and k_m can be obtained experimentally, by using numerical methods, or analytically in cases with simple geometries [5]. The expression used by Yigit and Christoforou [22] to predict the bending-shearing stiffness for a simply supported plate is $k_{bs} = D^*/(0.0116b^2)$, where b is

the smallest in-plane size of the plate [25, 29].

Using the equilibrium loads and considering a linear contact law, the simplified governing equation and the corresponding initial conditions for infinite plate behavior are:

$$\ddot{\alpha} + \frac{k_{\alpha}}{8\sqrt{I_1 D^*}} \dot{\alpha} + \frac{k_{\alpha}}{M_i} \alpha = 0 \quad ; \quad \alpha_0 = 0 \quad ; \quad \dot{\alpha}_0 = V_0 \quad (3)$$

where V_0 is the initial impactor velocity. Neglecting the terms k_m and M_p , the governing equation and the initial conditions for the quasi-static behavior are:

$$\left(1 + \frac{k_{\alpha}}{k_{bs}}\right) \ddot{\alpha} + \frac{k_{\alpha}}{M_i} \alpha = 0 \quad ; \quad \alpha_0 = 0 \quad ; \quad \dot{\alpha}_0 = \frac{k_{bs}}{k_{bs} + k_{\alpha}} V_0 \quad (4)$$

The mass-spring-damper model associated with the infinite plate behavior and described by the displacements of the impactor and of the plate, is shown in Fig. 2.a. The related simplified model which represents the governing equation Eq. (3) defined by the indentation and assuming a linear contact law, is schematized in Fig. 2.b. Likewise, in Fig. 3.a it is shown the corresponding model for the quasi-static impact behavior defined by the displacements of the impactor and of the plate. In addition, the model shown in Fig. 3.b also represents the quasi-static behavior according to the governing equation Eq. (4) which is defined by the indentation, the terms k_m and M_p are neglected, and assuming a linear contact law. The load terms are indicated in all the models shown in Figs. 2 and 3.

[Figure 2 about here.]

[Figure 3 about here.]

The governing equations can be expressed in a dimensionless framework which allows to reduce the number of the governing parameters into a set of suitable dimensionless parameters that provide more insight into the impact problem. The characterization diagram defines the system magnitudes as: mass $[\mathcal{M}] = M_i$, length $[\mathcal{L}] = \alpha_{max}$, and time

$[\mathcal{T}] = (k_\alpha^{-1}M_i)^{1/2}$. The term α_{max} is the maximum indentation and corresponds to the case where the global response of the plate is neglected, i.e., half-space behavior. Therefore, the expression of $\alpha_{max} = V_0 (k_\alpha^{-1}M_i)^{1/2}$ is simply found by equating all impact energy with the indentation energy.

Applying the dimensionless framework, the governing equations and the corresponding initial conditions for the infinite plate and the quasi-static behaviors are respectively:

$$\ddot{\bar{\alpha}} + 2\zeta_w \dot{\bar{\alpha}} + \bar{\alpha} = 0 \quad ; \quad \bar{\alpha}_0 = 0 \quad ; \quad \dot{\bar{\alpha}}_0 = 1 \quad (5)$$

$$(1 + \lambda^{-1}) \ddot{\bar{\alpha}} + \bar{\alpha} = 0 \quad ; \quad \bar{\alpha}_0 = 0 \quad ; \quad \dot{\bar{\alpha}}_0 = \lambda(1 + \lambda)^{-1} \quad (6)$$

where the over bar indicates dimensionless parameters. The terms

$\zeta_w = 1/16\sqrt{k_\alpha M_i/(I_1 D^*)}$ and $\lambda = k_{bs}/k_\alpha$ are the key characterization parameters. In the bibliography, the ζ_w ¹ parameter is called loss factor [2], relative plate mobility [3], or inelastic parameter [8, 26]. In addition, λ parameter is called relative stiffness. As suggested in the work developed by Olsson [3], the validity of Eq. (5) for rectangular plates with in-plane sizes $a > b$ and transverse isotropy is assured when $M_i/M_p \leq b/(\sqrt{2}\pi a)$, and for Eq. (6) when $M_i/M_p \geq 2$.

The solution of Eq. (5) depends on whether the characteristic equation has two conjugate complex roots ($\zeta_w < 1$), a double real root ($\zeta_w = 1$), or two different and real roots ($\zeta_w > 1$). The solution of Eq. (6) is:

$$\bar{\alpha}(\bar{t}) = \sqrt{\frac{\lambda}{1+\lambda}} \sin\left(\sqrt{\frac{\lambda}{1+\lambda}} \bar{t}\right) \quad (7)$$

¹In reference [2], the parameter ζ_w is noted as $\zeta = 2\zeta_w$. However, in references [3, 8, 26, 31, 32] the parameter ζ_w is noted as $\lambda = 2\zeta_w$, which is not the λ parameter written in the present paper.

Using the solutions of Eqs. (5) and (6) at contact times \bar{t} where the dimensionless indentation is maximized and knowing that $\bar{F}(\bar{t}) = \bar{\alpha}(\bar{t})$, a characterization diagram can be constructed as shown in Fig. 4. This diagram represents the variation of the maximum normalized impact force \bar{F}_{max} as a function of the relative mobility parameter ζ_w . The dashed curve which represents the infinite plate behavior is obtained from the solutions of Eq. (5), and the horizontal lines with different values of the relative stiffness λ are obtained using the solution described by Eq. (7).

[Figure 4 about here.]

Four different regions can be identified in the diagram. Impact configurations which define points in the right part of the diagram behave as quasi-static. For points which fall close to the dashed curve behave as infinite plate. Between the quasi-static and the infinite plate behaviors there is a transition zone where the resulting response is a combination of both behaviors. The curve which represents the boundary of the quasi-static response is obtained by $\bar{F}_b = \sqrt{\frac{0.68}{0.68 + \zeta_w^2}}$, as suggested in [22, 34]. Finally, the points that fall close to the maximum dimensionless force $\bar{F} = 1$ result in the half-space behavior, and can be obtained by setting in the simplified models $\zeta_w = 0$ or $\lambda \rightarrow \infty$.

In order to demonstrate the validity of the characterization diagram, several impact situations covering all behavior type regions were predicted by Yigit and Christoforou [22], by numerical integration of a complete analytical model which considers classical laminated plate theory, simply supported boundary conditions and a linear contact law. As shown in Fig. 4, the simulations follow reasonably well the trends of the characterization diagram, although in the transition zone, a complete analytical model is required in order to better describe the response.

3. Delamination threshold

Under drop-weight impact loading, the damage process starts with localized matrix cracks and fiber-matrix interfacial debondings which normally are not detectable neither by the impactor load cells used during impact tests nor using the typical NDI methods, e.g. ultrasonic techniques. It has been shown by Sjoblom et al. [35] that the presence of matrix cracks does not dramatically affect the overall laminate stiffness during an impact event. However, matrix crack tips act as initiation points for delaminations at interfaces between plies with different fiber orientations.

Delaminations are induced by interlaminar shear stresses which are promoted by matrix cracks, by stiffness mismatch between the adjacent plies, by ply clustering, and by the laminate deflection [36–38]. Increasing any of these factors will result in an increased mismatch in the bending deformations of adjacent ply groups with different orientations, yielding to large delaminations. Delaminations are a major threat because they are not detected by simple visual inspection and because they significantly reduce the compressive strength of the impacted structure.

The shape of the delamination is generally that of an oblong peanut, where its major axis follows the orientation of the lower ply at the interface [5, 8]. These shapes are a result of the shear stress distribution around the area surrounding the impactor, of the low interlaminar shear strength along or close to the direction of the fibers, and of the matrix cracks created by the flexural in-plane stresses [39].

There are two different phases during the impact driven delamination process. Firstly, when the impact force reaches a threshold value F_d , there is unstable crack propagation leading to instantaneous large delaminated areas. This often causes the impact force to drop in the response, indicating sudden loss of stiffness [40]. Secondly, the size of the delaminations increase linearly with the force indicating stable delamination growths [41]. The threshold load F_d does not physically represent the initiation of damage,

as sub-critical matrix cracks and small delaminations may initiate at lower forces. Rather, it represents the initial value at which a significant change in the stiffness properties of the laminate can be detected [36, 42]. Fig. 5 shows the typical history of the impact force for a monolithic laminated composite plate, where the threshold load F_d and the peak force F_{max} are identified. Depending on the impact velocity, F_d can be equal to F_{max} . On the other hand, the identification of F_d is not always clear, due to the effects of the governing parameters, or due to harmonic resonances of the impactor, of the load cell, or of the plate during the impact event.

[Figure 5 about here.]

A criterion for the growth of a single mid-plane circular delamination under static conditions was derived by Davies et al. [43]. The model is based on Linear Elastic Fracture Mechanics (LEFM) and assumes that mode II fracture determines delamination growth in a simply supported circular plate. To simplify the development of the model, static loading conditions were considered, the laminate was treated as isotropic, and only small deflections were considered (i.e. membrane effects are neglected). A more rigorous solution for an arbitrary number of delaminations n_d located at same intervals through-the-thickness of the plate was derived by Suemasu and Majima [44]. This criterion was also developed later by Olsson et al. [24]. The threshold is defined as:

$$F_{dn_d}^{stat} = \pi \sqrt{\frac{32D\mathcal{G}_{IIc}}{n_d + 2}} \quad (8)$$

where D is the bending stiffness, and \mathcal{G}_{IIc} is the fracture toughness in pure mode II. In the work developed by Olsson [25], Eq. (8) is used for orthotropic plates by simply changing the isotropic plate stiffness D by the effective plate stiffness D^* for orthotropic plates. Letting $n_d = 1$ (F_{d1}^{stat}), Eq. (8) yields to the criterion derived by Davies et al. [43]. Eq. (8) shows that delaminations grow under a constant load independently of the delamination

size. Therefore, an initial flaw is not required and thus the criterion can be used for the prediction of delamination onset. As can be checked, increasing the value of n_d , the load required to grow the delaminations decreases since the flexural stiffness of the plate is reduced. It is assumed that the first delamination appears when the impact force reach F_{d1}^{stat} , and sequentially, more delaminations appear on other interfaces [24]. In addition, experimental data and finite element simulations indicate that the delamination threshold load is independent of the boundary conditions and of the in-plane size of the plate [24, 25, 36]. Although the delamination criterion was derived assuming static loading conditions it may, with a moderate correction factor, be used for impact responses with dynamic effects, such as in an infinite plate behavior [24].

4. Selection of the impact configurations

The ASTM test method for measuring the damage resistance of a fiber-reinforced polymer matrix composite when subjected to a drop-weight impact event (i.e. ASTM D7136 / D7136M [42]) is taken as a reference in order to fix some of the governing parameters. Other guidelines for a drop-weight impact test provided by the aeronautical industry are available (e.g. Airbus AITM1-0010 [45]; Boeing 7260 [46]; NASA ST-1 [47]), however the set-ups are all essentially the same.

The standard is focused on rectangular, flat and monolithic laminated composite plates with 150mm×100mm in-plane dimensions. The specimens are placed over a flat support fixture base with a 125mm×75mm rectangular cut-out which allows the impactor to contact through the specimen without interferences (see Fig. 6.a). Guiding pins are located such that the specimen can be centrally positioned over the cut-out. The support fixture base has four rubber-tipped clamps which restrain the specimen during impact and provide a minimum holding capacity of 1100N. These rubber-tipped points clamp the specimen at 12.5mm and 6mm from each edge of the open window of the fixture base (see

Fig. 6.b) [45]. The boundary conditions provided by the edge supports can be approximated to simply supported [19].

[Figure 6 about here.]

Basically, the results obtained in the current impact tests are the impact force history and the initial impact velocity. In addition, the velocity and displacement history of the impactor, $V(t)$ and $w_i(t)$ respectively, can be calculated by integrating once and twice the force history [42]:

$$V(t) = V_0 + gt - \int_0^t \frac{F(t)}{M_i} dt \quad (9)$$

$$w_i(t) = V_0 t + \frac{gt^2}{2} - \int_0^t \left(\int_0^t \frac{F(t)}{M_i} dt \right) dt \quad (10)$$

where g is the acceleration due to the gravity. Additionally, the energy absorbed by the specimen, $E_a(t)$, can be calculated as:

$$E_a(t) = \frac{M_i (V_0^2 - V(t)^2)}{2} + M_i g w_i(t) \quad (11)$$

The stacking sequences proposed here to study the ply clustering effect are $[(45/0/-45/90)_4]_S$, $[(45_2/0_2/-45_2/90_2)_2]_S$, and $[45_4/0_4/-45_4/90_4]_S$ (in the following, these laminates are respectively identified as L1, L2, and L4). The plate stacking sequence is defined by taking the 0° fiber orientation aligned with the longer in-plane dimension of the plate. All laminates have the same plate thickness h because an equal number of plies is used (i.e. 32 plies; $h = 5.8\text{mm}$). However, the ply thicknesses h_p are different (i.e. L1: $h_p = h_{pp}$, L2: $h_p = 2h_{pp}$, and L4: $h_p = 4h_{pp}$, where h_{pp} is the thickness of a single pre-preg ply), yielding to different number of interfaces for delamination (i.e. L1: $n = 30$, L2: $n = 14$, and L4: $n = 6$). The plates were manufactured using Hexply AS4/8552

carbon-epoxy unidirectional pre-preg. The pre-preg was cut automatically and the lamination was done manually. The laminated plates were cured in an autoclave following the cycle specified by the supplier. The material properties are summarized in Table 1.

Three different impact energies E_i are considered: 19.3J, 28.6J, and 38.6J. Given that the impactor mass is kept constant at 5kg, the different energies also enable the study of the effects of velocity. Since the repeatability of the impact test is quite good, a sample of less than three specimens is used for some cases (two specimens for 19.3J: Lx -S1 and Lx -S2, one specimen for 28.6J: Lx -S3, and three specimens for 38.6J: from Lx -S4 to Lx -S6).

Using the material properties summarized in Table 1 and assuming that the effective in-plane dimensions of the plate are $a = 125\text{mm}$ and $b = 75\text{mm}$ (see Fig. 6.b), the resulting key parameters of the impact characterization diagram are: $\lambda = 1.62$ and $\zeta_w = 4.48$ for laminate L1, $\lambda = 1.60$ and $\zeta_w = 4.50$ for laminate L2, and $\lambda = 1.55$ and $\zeta_w = 4.58$ for laminate L4. Since the key parameters are independent of the impact velocity, the resulting values are constant for each laminate at any impact energy. Additionally, the key parameters are almost equal for all laminates due to the fact that the stiffness of the laminates is similar. Therefore, the dimensional elastic response of the laminates for each impact energy is also expected to be similar.

[Table 1 about here.]

Introducing the key parameters in the impact characterization diagram, a quasi-static behavior and a maximum dimensionless force of $\bar{F}_{max} = 0.78$ are predicted for all the laminates (see Fig. 4). Using the dimensionless framework, the maximum dimensional elastic force is obtained as: $F_{max} = \bar{F}_{max} V_0 \sqrt{M_i k_\alpha}$. Accordingly, the resulting values for each impact energy are: $F_{max} = 14.0\text{kN}$ for $E_i = 19.3\text{J}$, $F_{max} = 17.1\text{kN}$ for $E_i = 28.6\text{J}$, and $F_{max} = 19.8\text{kN}$ for $E_i = 38.6\text{J}$.

On the other hand, the values of the damage threshold for a mid-plane circular delamination predicted using Eq. (8) with $n = 1$ are: 8.53kN for laminate L1, 8.49kN for

laminate L2, and 8.34kN for laminate L4. These thresholds are constant for each impact energy since no dependence with velocity is considered in the formulation. As expected, the values obtained are practically the same for all laminates. In addition, the delamination occurrence is assured for all impact energies since the values of the peak load are greater than the delamination thresholds.

Finally, in order to assess the residual strength of the impacted specimens, the ASTM test method for measuring the compressive residual strength is taken as a reference, i.e., ASTM D7137 / D7137M [48]. This guideline is linked to the standard ASTM D7136 / D7136M [42] for drop-weight impact test. The standard proposes the fixture support sketched in Fig. 7.

[Figure 7 about here.]

5. Experimental results and discussion

The sequential tasks which were carried out in order to test the proposed lay-ups are: manufacturing of the specimens, NDI for the detection of manufacturing flaws, drop-weight impact tests, NDI to detect the BVID, and finally, CAI tests. The NDI before and after impact were performed by the C-scan ultrasonic technique. The inspections performed before impact are not shown because no initial flaws were observed.

All the impact tests described were carried out using a commercially available CEAST Fractovis Plus instrumented impact drop-weight tower. The impact tester is equipped with a load cell of 22kN attached to the impactor, an automatic pneumatic rebound brake system, and an edge support in accordance with the ASTM D7136 / D7136M [42] with a holding capacity of 3000N at each of the four clamping points.

All CAI tests were performed using an Instron-4208 electro-mechanic universal testing machine with a load cell of 300kN. The fixture support used follows the ASTM specifications (see Fig. 7).

5.1. Impact tests

5.1.1. Impact force versus time

In order to illustrate the excellent repeatability of the impact tests, Fig. 8 shows the evolutions of the impactor reaction force for repeated impact configurations of laminates L1 and L4. Therefore, for configurations with more than one specimen, the mean value is used in the following.

[Figure 8 about here.]

Figs. 9, 10, and 11 show the histories of the impactor reaction force for each impact energy of laminates L1, L2 and L4, respectively. An interesting observation is that the threshold load, F_d , at which significant loss of stiffness occurs, remains constant for each laminate independently of the impact energy. Therefore, F_d is independent of the impact velocity since the impactor mass is the same for all the energies defined. Moreover, as expected, the peak loads F_{max} and the slopes of the elastic regime increase by increasing the velocity, for all laminate types.

[Figure 9 about here.]

[Figure 10 about here.]

[Figure 11 about here.]

It is also observed that, increasing the velocity, the response is extended in time because the plate develops more damage. In other words, the impact time increases because the bending stiffness of the structure is reduced. This argument can be explained using the complete analytical models for the elastic prediction of the impact response. For instance, Fig. 12 shows the analytical predictions of laminate type L1 for the impact configurations with 19.3J and 38.6J energies. These predictions are obtained by using the

complete analytical impact model fed with the classical laminated plate theory and the Hertz contact law [49]. The number of modes considered for the Navier solution is 7 for each in-plane x and y directions, although the first mode alone is enough since the behaviors are quasi-static. As can be observed, the resulting elastic responses yield different slopes and peak loads, but the contact times are the same. Therefore, the experimental force histories show that when the velocity increases, larger damaged areas develop and so the impact contact duration increases.

[Figure 12 about here.]

Focusing again on Figs. 9, 10 and 11, the determination of the threshold loads for laminates L1 and L2 can be easily identified whereas for the laminate with the thickest plies, L4, this identification is more difficult. Moreover, the whole profiles of the force histories of laminate L4 do not have the large oscillations which occur for laminates L1 and L2. This fact indicates that changes in the stiffness during the impact are expected to be more progressive and smooth for laminates with thick plies than for laminates with thin plies. This behavior can be caused by the large matrix cracks which can occur when the plies are thick.

Despite the fact that all the laminate types considered have practically the same stiffness, the resulting impact force histories are clearly different from the point where significant damage starts. This is due to the differences in the ply thicknesses of the laminates, and further highlighted in Figs. 13, 14 and 15, which compare the results for the different laminates for each impact energy 19.3J, 28.6J and 38.6J. The first part of the results is the elastic regime of the impact process which is common for all laminates at each impact energy. However, the points where significant damage starts are clearly different, and from these points, the force histories separate and follow different paths.

Table 2 shows the differences in the threshold loads as well as in the peak loads for each impact energy. It can be observed that the predictions of F_d given by Eq. (8) are far

from the experimental values, especially for laminate L4. This result is due to the fact that the effect of the ply thickness is not accounted in the development of the load threshold, in addition, the assumption that a single delamination can generate a drop in the impact force history is not fully clear.

[Figure 13 about here.]

[Figure 14 about here.]

[Figure 15 about here.]

[Table 2 about here.]

Furthermore, Figs. 13, 14 and 15 show that the impact response is elongated by increasing the ply clustering of the laminate. Since delaminations cause a reduction of the stiffness, it is clear that larger delaminations should develop for laminate L4 because less interfaces are available for delamination in comparison with the other laminates.

5.1.2. *Impactor displacement, impactor velocity, and absorbed energy*

Fig. 16 shows the displacement and the velocity histories of all the laminates for an impact energy of 28.6J. As detected in the impact force histories, the displacement of L4 is the largest due to the reduced bending stiffness resulted from the large delamination areas induced during the impact. Accordingly, the velocity history of L4 is the slowest due to the same reason.

[Figure 16 about here.]

Using Eq. (11), the histories of the energy absorbed by the specimens $E_a(t)$ can be obtained. Figs. 17.a, 17.c and 17.e show these histories of each laminate type for each impact energy 19.3J, 28.6J and 38.6J, respectively. From these evolutions, it is possible to

know the dissipated energy by the specimen as it is indicated for laminate type L4 in Fig. 17.e. All these energies are summarized in Table 3. As can be observed, the dissipated energies for laminate L4 are slightly greater than the values of the other laminate types. However, it is reasonable to conclude that the energy dissipated is fairly independent of the laminate type. Moreover, as expected, the dissipated energies increase by increasing the velocity, for all laminate types.

[Table 3 about here.]

In addition, the impact force can be plotted as a function of the impactor displacement. These plots are shown in Figs. 17.b, 17.d and 17.f. It is clear that the area enclosed in these plots corresponds to the dissipated energy identified in the evolutions of the absorbed energy. For instance, Fig. 17.f indicates, in gray color, the corresponding energy dissipated by the laminate L4.

[Figure 17 about here.]

5.2. NDI: C-scan after impact

The ultrasonic C-scan inspections of the impacted laminates identify the projection of the delamination areas over the structure thickness. Therefore, the delaminations which are close to the impact face hide the existence of deeper delaminations. However, the delaminations are often larger as the interface is deeper in the laminate and they can usually be seen.

Generally, each delamination has the so-called peanut shape and the superposition of all these delaminations yields to a circular projected area. The proper interpretation of the through-the-thickness location of the delamination depends on the quality of the inspections performed. Fig. 18 shows a sample of the C-scan inspections of each laminate type for each impact energy.

[Figure 18 about here.]

It is observed that by increasing the impact velocity the projected area increases for all the laminates. This result correlates with the plots of the impact force histories shown previously (see Figs. 9, 10 and 11), where the responses are extended in time when the velocity is increased due to the reduction of the bending stiffness as a consequence of the damage developed.

In addition, by reducing the number of interfaces available for delamination, the resulting projected delamination area is increased as the dissipated energies are similar (see Table 3). This result is also related to the impact force histories (see Figs. 13, 14 and 15), where the responses for laminate type L4 are larger since the bending stiffnesses are reduced due to the large delaminations created.

The shapes of the projected delamination areas are clearly different for each laminate type. The shape of laminates L1 follow a quite similar circular pattern at each impact energy. Likewise, the shapes of laminate type L2 are also fairly circular, although in contrast with laminate L1, a narrow and elongated delamination appears at the deepest interface which is more evident for the highest impact energy. Finally, the delamination shapes of laminate type L4 significantly differ from the other laminates. The areas are very large, especially in the deeper interfaces, and their shapes and locations through-the-thickness can be easily recognized.

It is important to point out that the growth of delaminations can be affected by the finite in-plane dimensions of the plates, the stacking sequences, the impactor mass and velocity, and the edge supports. All the impact configurations and stacking sequences tested are in agreement with the recommendations suggested by ASTM D7136 / D7136M [42]. The standard remarks that if all the recommendations are followed, the maximum delamination diameter will be less than half of the unsupported specimen width (38mm). However, most of the delamination areas obtained are greater than this value.

Laminate type L4 has fewer interfaces for delamination than laminates L1 and L2. As such, the energy is dissipated by means of large damage areas which could be stopped by the membrane effects and/or the edge supports. The larger delaminations generated by ply clustering result in larger deflections and associated stronger membrane effects, which are known to suppress delamination growth [25]. This is suggested by the relation between the projected delamination areas and the impact energy, as shown in Fig. 19, where the fitting line of laminate type L4 has the lowest slope. Furthermore, since the delaminations cannot grow, the energy must be dissipated by other means, such as large indentation and fiber breakage.

[Figure 19 about here.]

Since the C-scan inspections provide the projected delamination area at the end of the impact tests, these results do not reveal clearly whether the critical point F_d corresponds to the generation of a single delamination or a set of delaminations. In this sense, finite element simulations of the impact tests can be performed to provide additional information on this phenomenon. This will be the subject of future work.

Olsson et al. [24] formulated a threshold load for the growth of an arbitrary number of circular delaminations located at same intervals through-the-thickness of a circular plate (see Eq. (8)). Based on this work, a new criterion can be developed assuming that n_d^* delaminations can grow, but now counted from the back face of the plate and generating n_d^* sub-laminates with a thickness equal to the clustering thickness h_p (see Fig. 20). This approach is relevant for cases that suffer the largest delaminations at the deeper interfaces of the laminate, such as it occurs for laminate type L4 (see Fig. 18). The relationship between the out-of-plane displacement w_o and an external point load $F_{n_d^*}^{stat}$ is given by the theory for thin plates as:

$$w_o = \frac{r_p^2}{16\pi D^*} F_{n_d^*}^{stat} \quad (12)$$

where r_p is the radius of the plate. Assuming that the system is linear, it allows to apply the principle of superposition for the development of the elastic energy of a plate with n_d^* circular delaminations of radius a_c :

$$U = \frac{r_p^2 \left(F_{n_d^*}^{stat}\right)^2}{32\pi D^*} - \frac{a_c^2 \left(F_{n_d^*}^{stat}\right)^2}{32\pi D^*} + \frac{a_c^2 h^3 \left(F_{n_d^*}^{stat}\right)^2}{32\pi D^* \left(\left(h - n_d^* h_p\right)^3 + n_d^* h_p^3\right)} \quad (13)$$

The first term in the right-hand side of Eq. (13) is the elastic energy of the plate without delaminations. The second term is the energy of a circular plate of radius a_c . The last term is related to the elastic energy of the circular plate portions of radius a_c (see Fig. 20). Knowing that $\frac{\partial U}{\partial a_c} = 2\pi a_c \mathcal{G}_{IIc}$, the threshold load results:

$$F_{n_d^*}^{stat} = 4\pi \sqrt{2D^* \mathcal{G}_{IIc}} \left(-1 + \frac{h^3}{\left(h - n_d^* h_p\right)^3 + n_d^* h_p^3} \right)^{-\frac{1}{2}} \quad (14)$$

[Figure 20 about here.]

As occurs with the criterion defined by Eq. (8), the threshold $F_{n_d^*}^{stat}$ does not depend on the initial crack length of the n_d^* delaminations so it can be interpreted as a criterion for delamination onset. Increasing the value of n_d^* , the load required to grow the delaminations decreases since the flexural stiffness of the plate is reduced. Table 4 summarizes the values of $F_{n_d^*}^{stat}$ which are closer to the experimental values for each laminate type. The general trend is that practically all the interfaces available for delamination, starting from the mid-plane and ending at the back face of the plate, will delaminate at the critical point F_d . The proposed threshold should be understood qualitatively, since the delaminations are assumed perfectly circular and equal effective flexural stiffness D^* is assumed for all sub-laminates.

[Table 4 about here.]

5.3. CAI tests

Not a single CAI test performed experienced unacceptable damage modes, such as those related to load introduction by the support fixture. Table 3 summarizes the mean residual compressive loads F_{fc} obtained for each laminate. It is observed that increasing the impact energy (or the impact velocity), the residual compressive loads are reduced for all the laminates tested.

In addition, the damage tolerance estimated by means of the residual compressive load does not seem to be reduced by increasing the ply thickness, because all laminate types show similar values of the residual compressive load at each impact energy (except for specimen L4-S1). This result is due to the fact that the compressive load depends on a combination of variables such as the number of delamination planes, the size of the delaminations, and their locations through-the-thickness of the laminate. However, more tests are needed in order to further support these conclusions since the repeatability of the CAI tests is not as good as in the impact tests.

6. Conclusions

The analytical impact models for the prediction of the elastic response are a powerful tool to define a suitable test matrix of specimens, to obtain a preliminary qualitative understanding of the effects of the governing parameters on the impact response, and to interpret the experimental results obtained. The analytical impact models are completed with analytical thresholds for the prediction of the damage mechanisms that can occur in a laminated composite plate under drop-weight impact loading. Under these impacts, the most critical damage mode is delamination.

It is concluded that increasing the impact velocity, the slope of the load-time relation in the elastic regime as well as the maximum impact force are increased, as predicted by

means of the analytical impact models. However, the threshold load, F_d , remains constant for different impact velocities. In addition, by increasing the velocity the response is extended in time because the plate develops more damage.

Increasing ply clustering the values of F_d and F_{max} are reduced under equal impact conditions. Additionally, by increasing ply clustering the changes in the stiffness during the impact become more progressive and smooth when compared with laminates with thin plies. This result implies difficulties in the detection of F_d for laminates with thick plies.

It has been also shown that increasing the number of clustered plies, the response is elongated in time. This result is related with the fact that larger delaminations are created when the number of interfaces available for delamination is reduced. Therefore, it can be concluded that ply clustering results in a lower damage resistance of a composite structure.

However, the damage tolerance, quantified using the residual compressive load, is unaffected by increasing the ply thickness, because all the laminate types presented have shown similar values of peak compressive loads at each impact energy.

Relevant future work would be to perform impact tests with impact energies which generate maximum impact loads similar to the experimental threshold values. The goal would be to verify experimentally the damage mechanisms that generate the first load drop, if it occurs, in the evolution of the impact force. In this sense, it is necessary to use NDI techniques which can offer 3D views of the post-impact damage, such as X-ray computerized tomography. In addition, finite element simulations of the impact tests would be performed to provide additional information on this phenomenon. Accordingly, the suitability of the analytical damage thresholds can be analyzed in more detail, so new improved proposals can be developed.

7. Acknowledgments

This work has been partially funded by the Spanish Government (Ministerio de Ciencia e Innovacin) under contracts MAT2009-07918 (subprogram MAT) and DPI2009-08048. The first author would like to thank the Generalitat de Catalunya for the FI pre-doctorate grant supported by European Social funds. The third author would like to thank the financial support of the Portuguese Foundation for Science and Technology (FCT) under the project PDCT / EMEPME / 64984 / 2006. Finally, the authors would like to thank the reviewers of the journal of Composites Science and Technology for their positive comments that have helped to improve the paper.

References

- [1] M. O. W. Richardson, M. J. Wisheart, Review of low-velocity impact properties of composite materials, *Composites Part A-Applied Science and Manufacturing* 27 (12) (1996) 1123–1131.
- [2] A. P. Christoforou, A. S. Yigit, Characterization of impact in composite plates, *Composite Structures* 43 (1) (1998) 15–24.
- [3] R. Olsson, Mass criterion for wave controlled impact response of composite plates, *Composites Part A-Applied Science and Manufacturing* 31 (8) (2000) 879–887.
- [4] R. Olsson, Impact response of composite laminates - a guide to closed form solutions, FFA-TN 1992-33, Bromma: The Aeronautical Research Institute of Sweden (1993).
- [5] G. A. O. Davies, R. Olsson, Impact on composite structures, *The Aeronautical Journal* 108 (2004) 541–563.
- [6] R. Olsson, Closed form prediction of peak load and delamination onset under small mass impact, *Composite Structures* 59 (3) (2003) 341–349.
- [7] A. P. Christoforou, Impact dynamics and damage in composite structures, *Composite Structures*, 52 (2) (2001) 181–188.
- [8] S. Abrate, *Impact on composite structures*, Cambridge University Press, UK, 1998.
- [9] G. A. O. Davies, X. Zhang, G. Zhou, S. Watson, Numerical modelling of impact damage, *Composites* 25 (5) (1994) 342–350.
- [10] D. J. Elder, R. S. Thomson, M. Q. Nguyen, M. L. Scott, Review of delamination predictive methods for low speed impact of composite laminates, *Composite Structures* 66 (1-4) (2004) 677–683.
- [11] M. R. Wisnom, B. Khan, S. R. Hallett, Size effects in unnotched tensile strength of unidirectional and quasi-isotropic carbon/epoxy composites, *Composite Structures* 84 (1) (2008) 21–28.
- [12] B. G. Green, M. R. Wisnom, S. R. Hallett, An experimental investigation into the tensile strength scaling of notched composites, *Composites Part A: Applied Science and Manufacturing* 38 (3) (2007) 867–878.
- [13] M. R. Wisnom, S. R. Hallett, The role of delamination in strength, failure mechanism and hole size effect in open hole tensile tests on quasi-isotropic laminates, *Composites Part A: Applied Science and Manufacturing* 40 (4) (2009) 335–342.
- [14] M. R. Wisnom, S. R. Hallett, C. Soutis, Scaling effects in notched composites, *Journal of Composite Materials* 44 (2) (2010) 195–210.
- [15] P. Viot, L. Ballre, L. Guillaumat, J.-L. Lataillade, Scale effects on the response of composite

- structures under impact loading, *Engineering Fracture Mechanics* 75 (9) (2008) 2725-2736.
- [16] A. Parvizi, K. W. Garrett, J. E. Bailey, Constrained cracking in glass fibre-reinforced epoxy cross-ply laminates, *Journal of Materials Science* 13 (1) (1978) 195–201.
- [17] G. J. Dvorak, N. Laws, Analysis of progressive matrix cracking in composite laminates - II. First ply failure., *Journal of Composite Materials* 21 (4) (1987) 309–329.
- [18] R. Prinz, L. Cao, Analysis of strain-energy-release rates for unidirectional graphite/epoxy laminates with separated central plies under fatigue loading. Proceedings of Seventh International Conference on Composite Materials: ICCM-VII. Beijing, China, 1989, pp. 1–6.
- [19] E. Fuoss, P. V. Straznický, C. Poon, Effects of stacking sequence on the impact resistance in composite laminates - Part 1: Parametric study, *Composite Structures* 41 (1) (1998) 67–77.
- [20] C. S. Lopes, P. P. Camanho, Z. Gürdal, P. Maimí, E. V. González, Low-velocity impact damage on dispersed stacking sequence laminates. Part II: Numerical simulations, *Composites Science and Technology* 69 (7-8) (2009) 937–947.
- [21] C. S. Lopes, O. Seresta, Y. Coquet, Z. Gürdal, P. P. Camanho, B. Thuis, Low-velocity impact damage on dispersed stacking sequence laminates. Part I: Experiments, *Composites Science and Technology* 69 (7-8) (2009) 926–936.
- [22] A. S. Yigit, A. P. Christoforou, Limits of asymptotic solutions in low-velocity impact of composite plates, *Composite Structures* 81 (4) (2007) 568–574.
- [23] A. P. Christoforou, A. S. Yigit, Effect of flexibility on low velocity impact response, *Journal of Sound and Vibration*, 217 (3) (1998) 563–578.
- [24] R. Olsson, M. V. Donadon, B. G. Falzon, Delamination threshold load for dynamic impact on plates, *International Journal of Solids and Structures* 43 (10) (2006) 3124–3141.
- [25] R. Olsson, Analytical prediction of large mass impact damage in composite laminates, *Composites Part A-Applied Science and Manufacturing* 32 (9) (2001) 1207–1215.
- [26] S. Abrate, Modeling of impacts on composite structures, *Composite Structures* 51 (2) (2001) 129–138.
- [27] C. Lin, M. S. H. Fatt, Perforation of composite plates and sandwich panels under quasi-static and projectile loading, *Journal of Composite Materials* 40 (20) (2006) 1801–1840.
- [28] A. S. Yigit, A. P. Christoforou, On the impact of a spherical indenter and an elastic-plastic transversely isotropic half-space, *Composites Engineering*, 4 (11) (1994) 1143–1152.
- [29] J. N. Reddy, *Theory and analysis of elastic plates and shells*, Taylor and Francis, Philadelphia, 2007.
- [30] R. W. Clough, J. Penzien, *Dynamics of structures*, McGraw-Hill, New York, 1993.

- [31] C. Zener, The intrinsic inelasticity of large plates, *Physical Review* 59 (8) (1941) 669–673.
- [32] R. Olsson, Impact response of orthotropic composite plates predicted from a one-parameter differential equation, *AIAA journal* 30 (6) (1992) 1587–1596.
- [33] K. N. Shivakumar, W. Elber, W. Illg, Prediction of impact force and duration due to low-velocity impact on circular composite laminates, *Journal of Applied Mechanics* 52 (3) (1985) 674–680.
- [34] S. R. Swanson, Limits of quasi-static solutions in impact of composite structures, *Composites Engineering* 2 (4) (1992) 261–267.
- [35] P. O. Sjoblom, J. T. Hartness, T. M. Cordell, On low-velocity impact testing of composite materials, *Journal of Composite Materials* 22 (1) (1988) 30–52.
- [36] G. A. Schoepner, S. Abrate, Delamination threshold loads for low velocity impact on composite laminates, *Composites Part A: Applied Science and Manufacturing* 31 (9) (2000) 903–915.
- [37] D. Liu, Impact-induced delamination - a view of bending stiffness mismatching, *Journal of Composite Materials* 22 (7) (1988) 674–692.
- [38] H. Morita, T. Adachi, Y. Tateishi, H. Matsumoto, Characterization of impact damage resistance of CF/PEEK and CF/toughened epoxy laminates under low and high velocity impact tests, *Journal of Reinforced Plastics and Composites* 16 (2) (1997) 131–143.
- [39] G. A. O. Davies, X. Zhang, Impact damage prediction in carbon composite structures, *International Journal of Impact Engineering* 16 (1) (1995) 149–170.
- [40] X. Zhang, Impact damage in composite aircraft structures experimental testing and numerical simulation, *Proceedings of the Institution of Mechanical Engineers, Part G: Journal of Aerospace Engineering* 212 (4) (1998) 245–259.
- [41] W. C. Jackson, C. C. Poe, Use of impact force as a scale parameter for the impact response of composites laminates, *Journal of Composites Technology and Research* 15 (4) (1993) 282–289.
- [42] ASTM D 7136/D 7136M-05, Standard Test Method for Measuring the Damage Resistance of a Fiber-Reinforced Polymer Matrix Composite to a Drop-Weight Impact Event. ASTM International. West Conshohocken PA, USA (2005).
- [43] G. A. O. Davies, P. Robinson, Predicting failure by debonding delaminations, In: *debonding/delamination of composites*, AGARD-CP-530, Advisory Group for Aerospace Research and Development, Neuilly Sur Seine (1992).
- [44] H. Suemasu, O. Majima, Multiple delaminations and their severity in circular axisymmetric plates subjected to transverse loading, *Journal of Composite Materials* 30 (4) (1996) 441–453.

- [45] AITM1-0010, Airbus Test Method. Fibre Reinforced Plastics: Determination of Compression Strength After Impact. Blagnac Cedex, France (2005).
- [46] BSS-7260, Boeing Specification Support Standard: Advanced Composite Compression Tests. The Boeing Company, Seattle, Washington (1988).
- [47] NASA ST-1, Standard test for toughened resin composites, Tech. Rep. 1092 (1982).
- [48] ASTM D 7137/D 7137M-05, Standard Test Method for Compressive Residual Strength Properties of Damaged Polymer Matrix Composite Plates. ASTM International. West Conshohocken PA, USA (2005).
- [49] T. M. Tan, C. T. Sun, Use of statical indentation laws in the impact analysis of laminated composite plates, *Journal of Applied Mechanics* 52 (1) (1985) 6–12.

List of Figures

1	Impact responses (after Olsson [4]): (a) dominated by dilatational waves, (b) dominated by flexural and shear waves, and (c) quasi-static response.	33
2	Lumped-mass models for infinite plate impact behavior, (a) defined by the displacements of the impactor and of the plate (after Olsson [4]), and (b) by the indentation, with $q = 1$	34
3	Lumped-mass models for quasi-static impact behavior, (a) defined by the displacements of the impactor and of the plate (after Shivakumar et al. [33]), and (b) simplified by the indentation, with $q = 1$	35
4	Impact characterization diagram (after Yigit and Christoforou [22]): dimensionless maximum force \bar{F}_{max} versus relative mobility ζ_w . The x-mark depicted corresponds to the point of the impact configurations considered for the analysis of the ply clustering effect.	36
5	Representative history of the impact force [42].	37
6	(a) Impact support fixture (after Fuoss et al. [19]); (b) detail of the support area and clamping points of the specimen.	38
7	(a) CAI support fixture and (b) the corresponding constraints.	39
8	Impact force histories of laminates (a-b) L1 and (c-d) L4.	40
9	Impact force histories of laminate L1 for each impact energy (black: 19.3J; gray: 28.6J; dashed: 38.6J).	41
10	Impact force histories of laminate L2 for each impact energy (black: 19.3J; gray: 28.6J; dashed: 38.6J).	42
11	Impact force histories of laminate L4 for each impact energy (black: 19.3J; gray: 28.6J; dashed: 38.6J).	43
12	Experimental and analytical impact force histories of laminate L1 for 19.3J and 38.6J impact energies.	44
13	Impact force histories for 19.3J of laminates L1 (black), L2 (gray), and L4 (dashed).	45
14	Impact force histories for 28.6J of laminates L1 (black), L2 (gray), and L4 (dashed).	46
15	Impact force histories for 38.6J of laminates L1 (black), L2 (gray), and L4 (dashed).	47
16	Impactor (a) displacements and (b) velocities of all the laminates for 28.6J energy.	48
17	Evolution of the (a,c,e) absorbed energy and (b,d,f) impact force versus impactor displacement of each laminate type.	49
18	Sample of C-scan inspections of laminates L1, L2 and L4.	50
19	Projected delamination areas in function of the impact energy.	51
20	Example of back face delaminations.	52

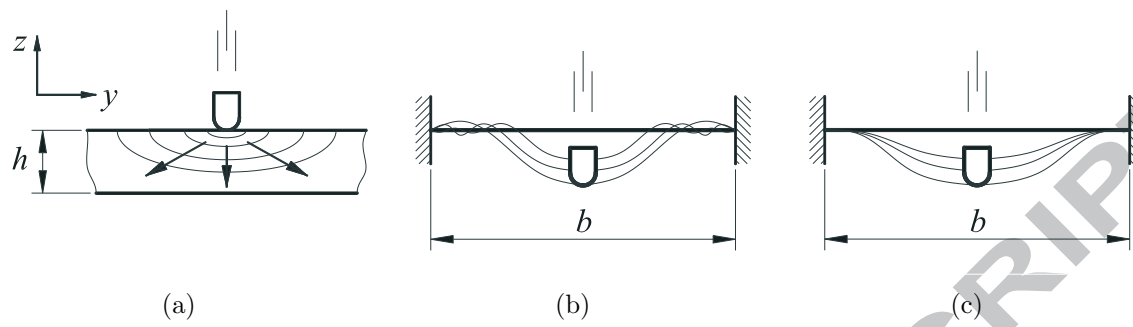


Figure 1: Impact responses (after Olsson [4]): (a) dominated by dilatational waves, (b) dominated by flexural and shear waves, and (c) quasi-static response.

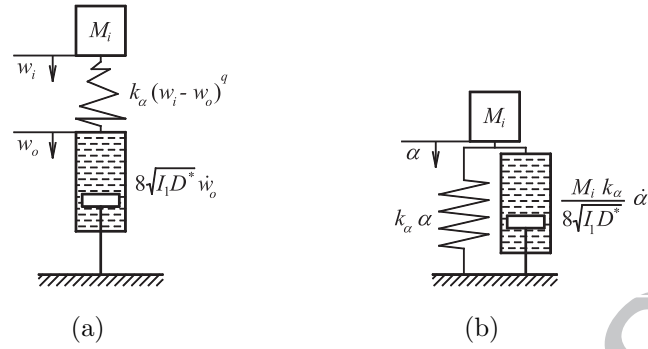


Figure 2: Lumped-mass models for infinite plate impact behavior, (a) defined by the displacements of the impactor and of the plate (after Olsson [4]), and (b) by the indentation, with $q = 1$.

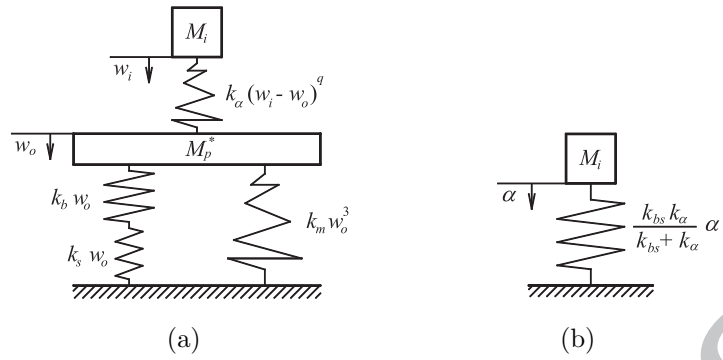


Figure 3: Lumped-mass models for quasi-static impact behavior, (a) defined by the displacements of the impactor and of the plate (after Shivakumar et al. [33]), and (b) simplified by the indentation, with $q = 1$.

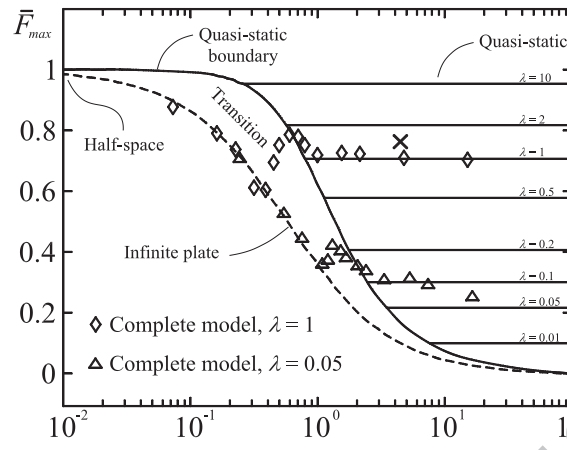


Figure 4: Impact characterization diagram (after Yigit and Christoforou [22]): dimensionless maximum force \bar{F}_{max} versus relative mobility ζ_w . The x-mark depicted corresponds to the point of the impact configurations considered for the analysis of the ply clustering effect.

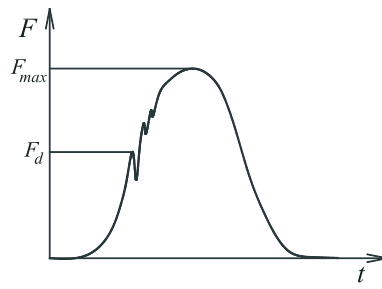


Figure 5: Representative history of the impact force [42].

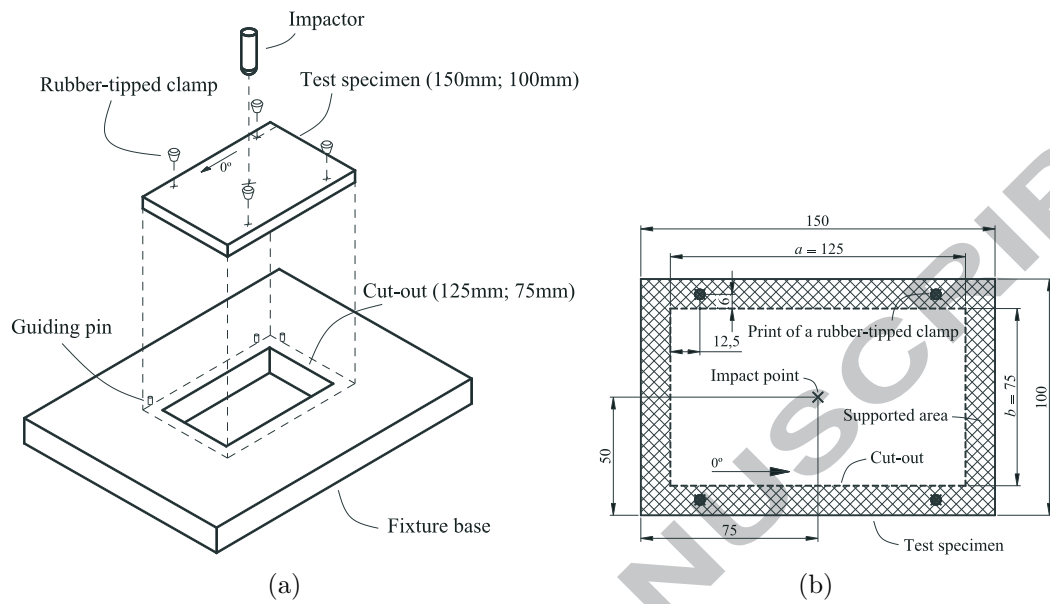


Figure 6: (a) Impact support fixture (after Fuoss et al. [19]); (b) detail of the support area and clamping points of the specimen.

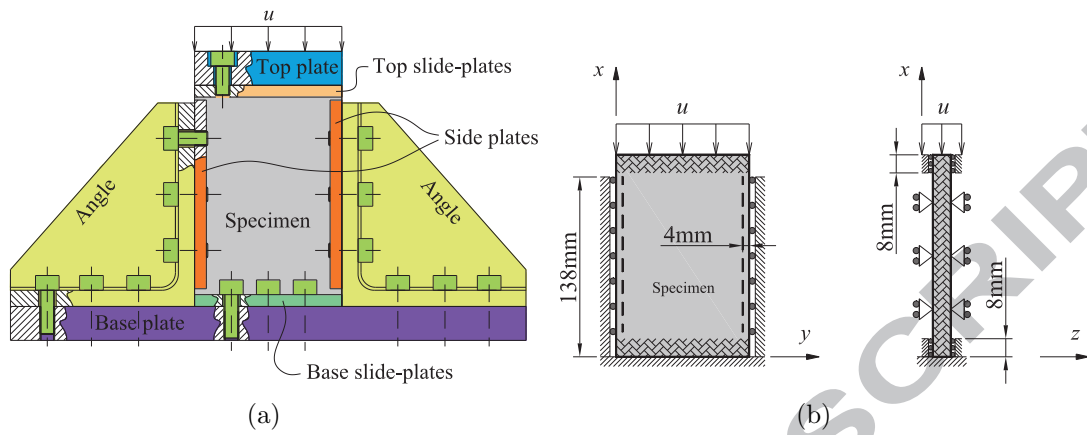


Figure 7: (a) CAI support fixture and (b) the corresponding constraints.

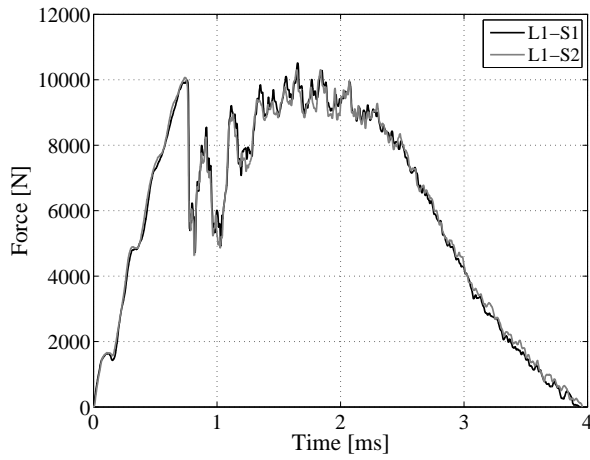
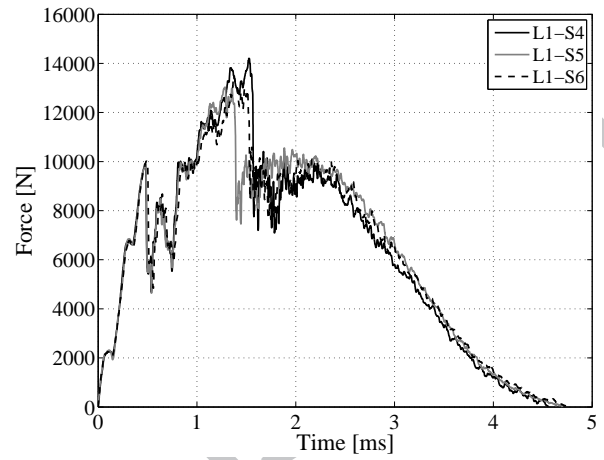
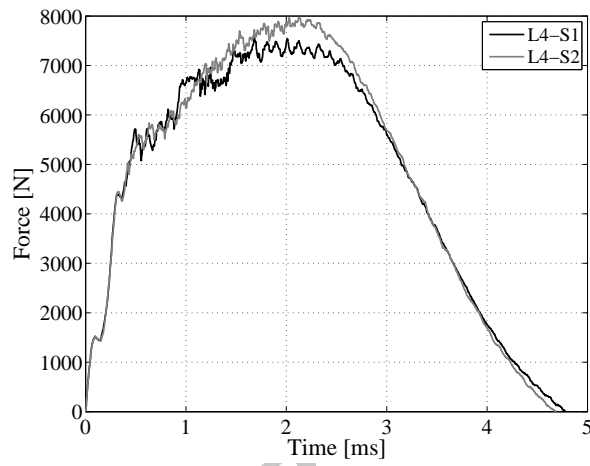
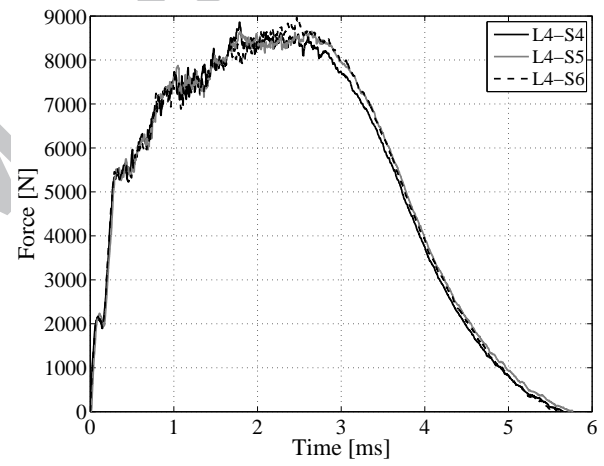
(a) $E_i = 19.3\text{J}$ and $M_i = 5\text{kg}$.(b) $E_i = 38.6\text{J}$ and $M_i = 5\text{kg}$.(c) $E_i = 19.3\text{J}$ and $M_i = 5\text{kg}$.(d) $E_i = 38.6\text{J}$ and $M_i = 5\text{kg}$.

Figure 8: Impact force histories of laminates (a-b) L1 and (c-d) L4.

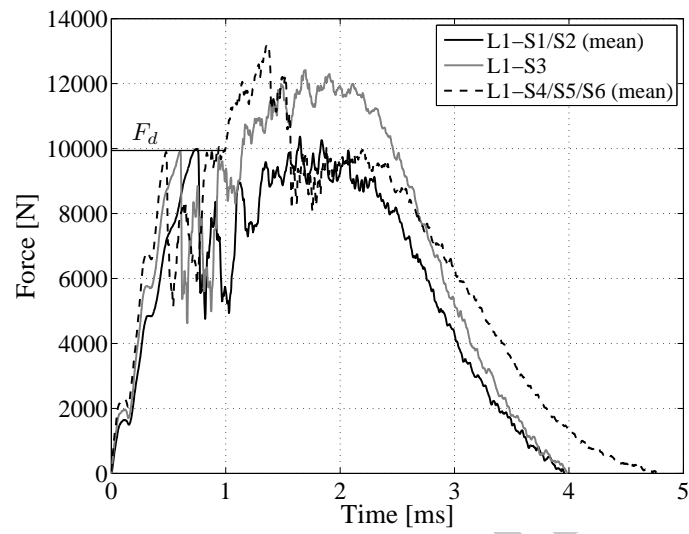


Figure 9: Impact force histories of laminate L1 for each impact energy (black: 19.3J; gray: 28.6J; dashed: 38.6J).

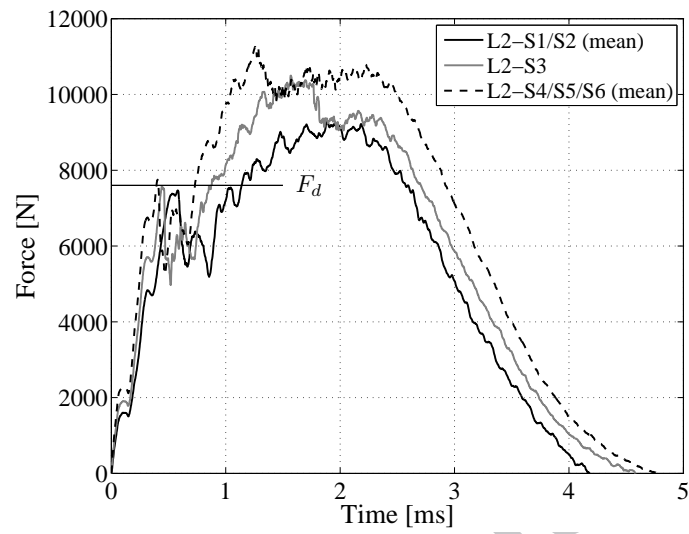


Figure 10: Impact force histories of laminate L2 for each impact energy (black: 19.3J; gray: 28.6J; dashed: 38.6J).

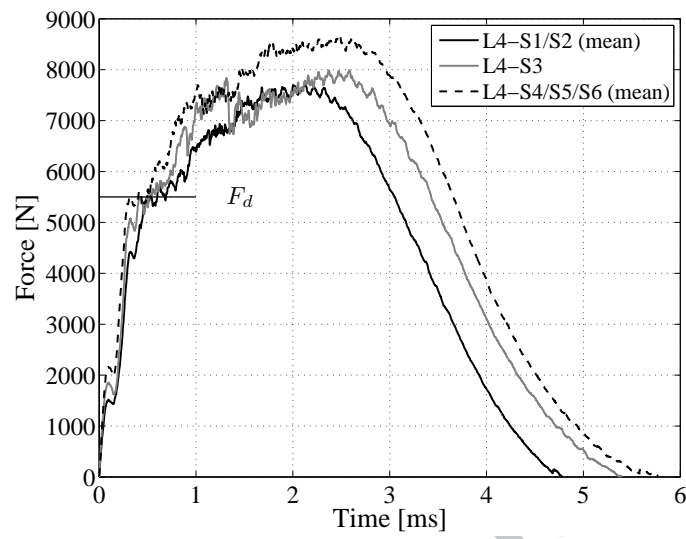


Figure 11: Impact force histories of laminate L4 for each impact energy (black: 19.3J; gray: 28.6J; dashed: 38.6J).

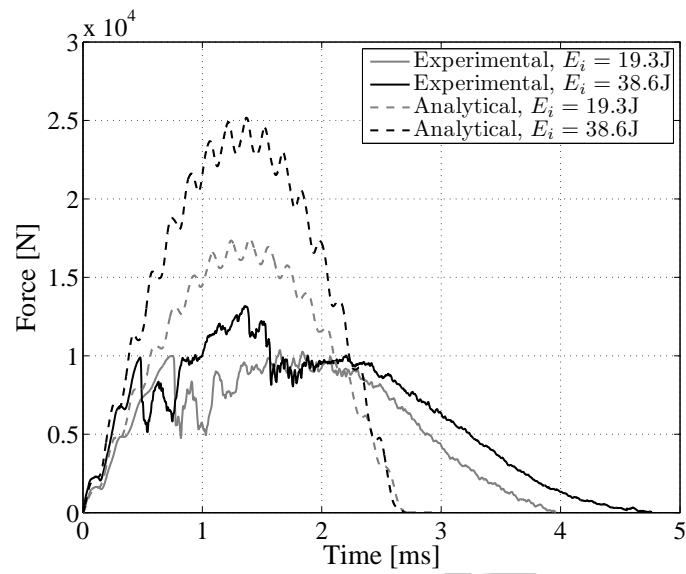


Figure 12: Experimental and analytical impact force histories of laminate L1 for 19.3J and 38.6J impact energies.

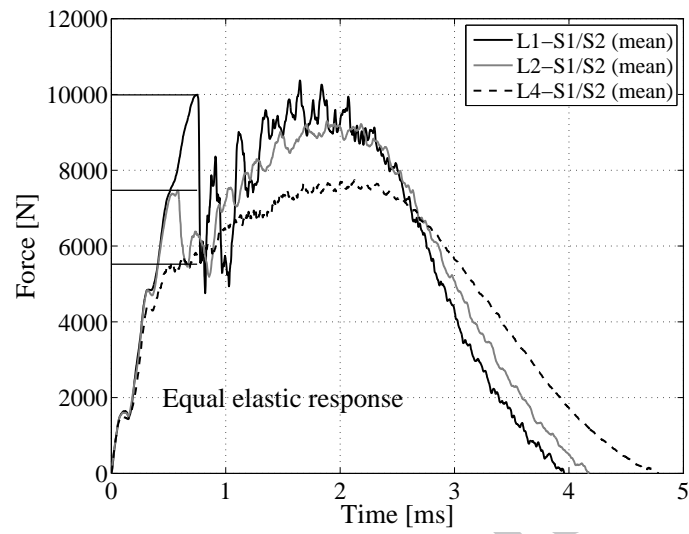


Figure 13: Impact force histories for 19.3J of laminates L1 (black), L2 (gray), and L4 (dashed).

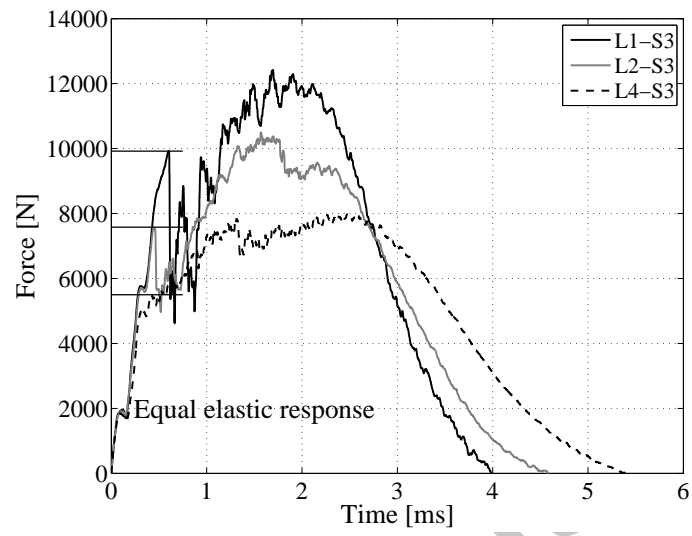


Figure 14: Impact force histories for 28.6J of laminates L1 (black), L2 (gray), and L4 (dashed).

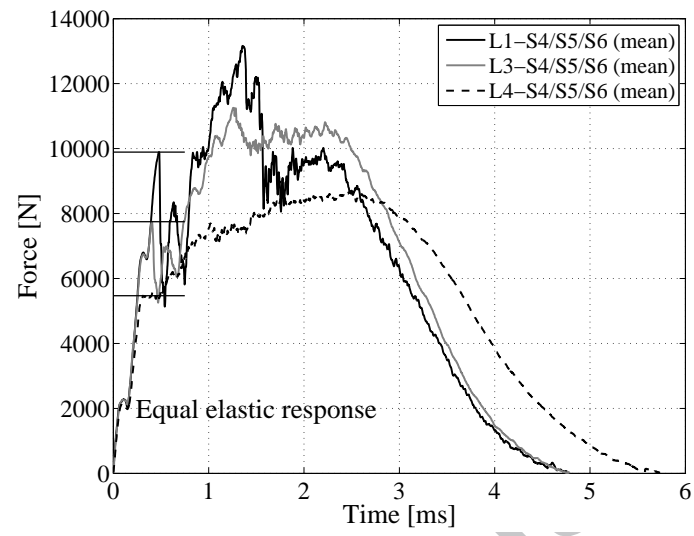


Figure 15: Impact force histories for 38.6J of laminates L1 (black), L2 (gray), and L4 (dashed).

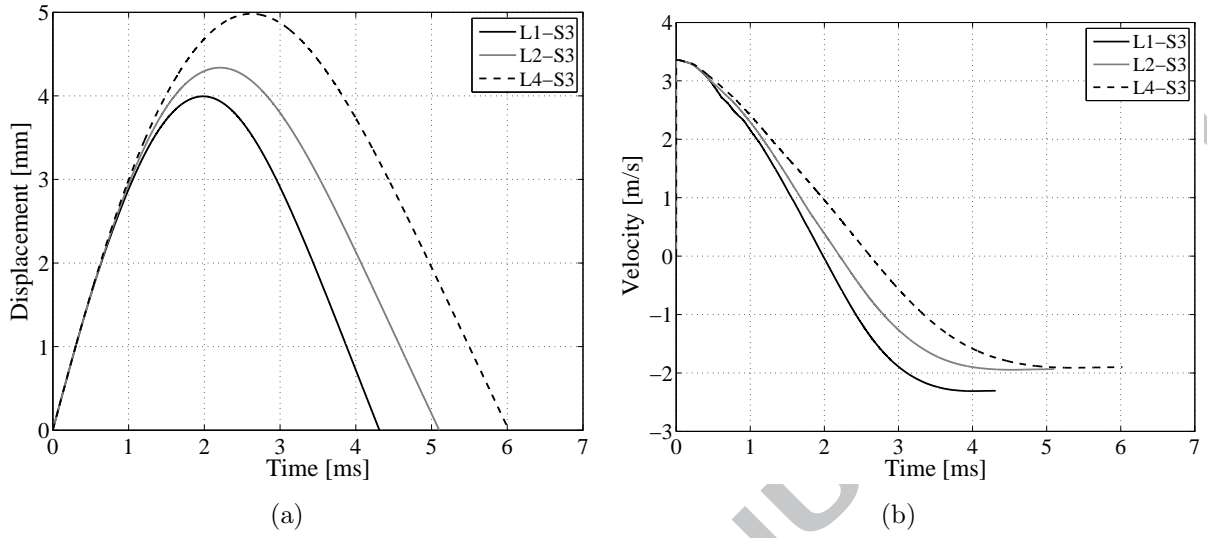


Figure 16: Impactor (a) displacements and (b) velocities of all the laminates for 28.6J energy.

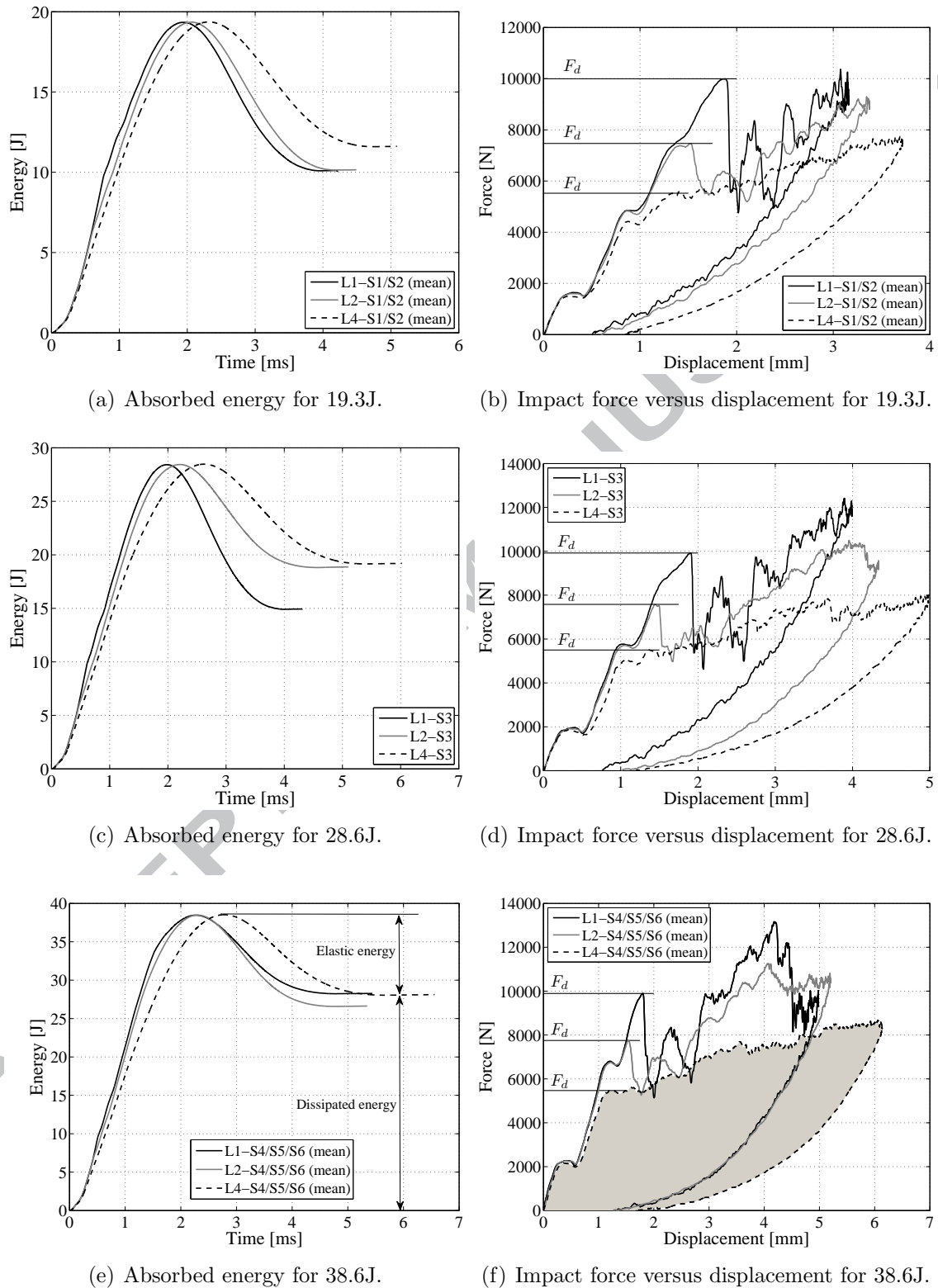


Figure 17: Evolution of the (a,c,e) absorbed energy and (b,d,f) impact force versus impactor displacement of each laminate type.

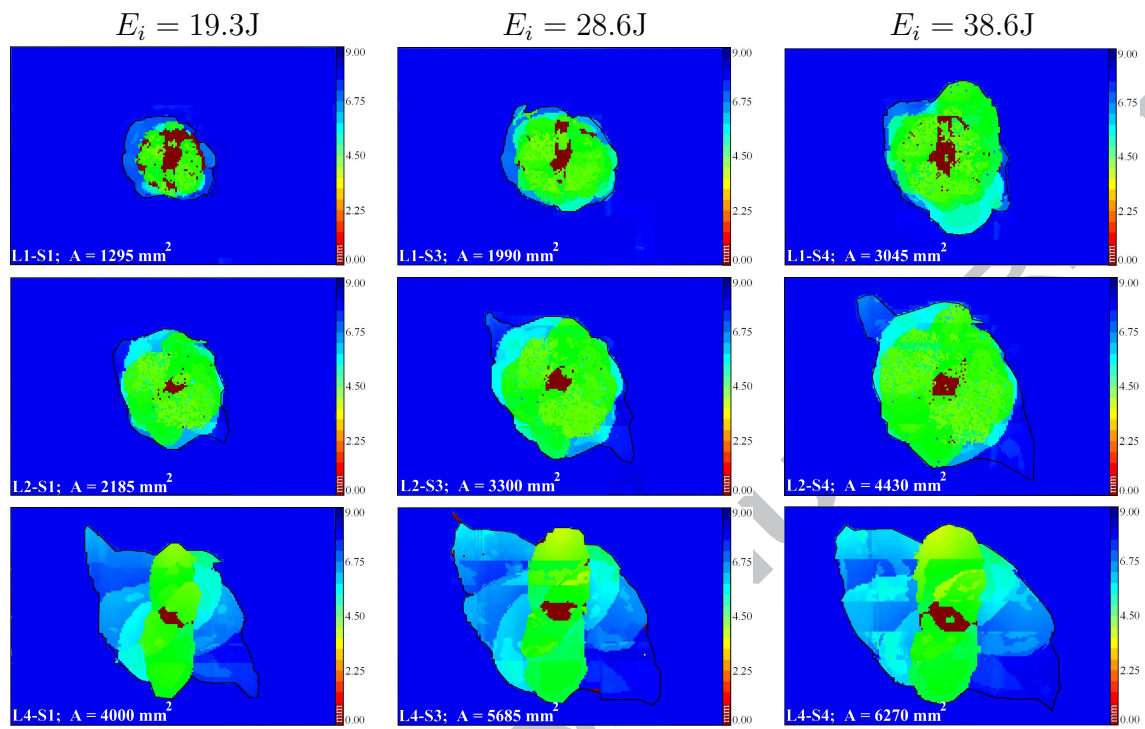


Figure 18: Sample of C-scan inspections of laminates L1, L2 and L4.

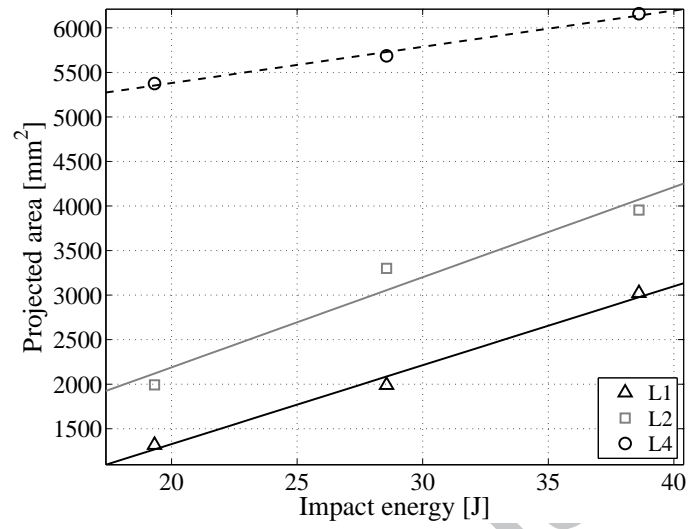


Figure 19: Projected delamination areas in function of the impact energy.

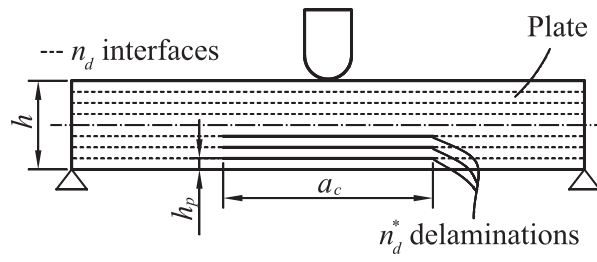


Figure 20: Example of back face delaminations.

List of Tables

1	Hexply AS4/8552 properties.	54
2	Experimental threshold loads F_d and peak loads F_{max}	55
3	Absorbed energies E_a and residual compressive loads F_{fc} of all laminates for each impact energy (in Joules).	56
4	Values of $F_{n_d}^{stat}$ to generate n_d^* sub-laminates counted from the back face of the plate.	57

Table 1: Hexply AS4/8552 properties.

Density	$1590 \times 10^{-9} \text{kg/mm}^3$
Elastic properties	$E_{11} = 128.0 \text{GPa}; E_{22} = 7.6 \text{GPa};$ $G_{12} = 4.4 \text{GPa}; \nu_{12} = 0.35; \nu_{23} = 0.45$
Compressive strength	$Y_C = 199.8 \text{MPa}$
Fracture toughness in pure mode II	$\mathcal{G}_{IIc} = 0.79 \text{N/mm}$

Table 2: Experimental threshold loads F_d and peak loads F_{max} .

Laminate	Energy [J]:	Threshold loads F_d [kN]				Energy [J]:	Peak loads F_{max} [kN]		
		19.3 (mean)	28.6	38.6 (mean)	Mean		19.3 (mean)	28.6	38.6 (mean)
L1	9.99	9.92	9.89	9.94	10.41	12.42	13.57		
L2	7.47	7.58	7.75	7.60	9.34	10.50	11.37		
L4	5.52	5.50	5.47	5.50	7.78	8.00	8.83		

Table 3: Absorbed energies E_a and residual compressive loads F_{fc} of all laminates for each impact energy (in Joules).

Laminate	$E_i = 19.3\text{J}$		$E_i = 28.6\text{J}$		$E_i = 38.6\text{J}$	
	E_a [J]	F_{fc} [kN]	E_a [J]	F_{fc} [kN]	E_a [J]	F_{fc} [kN]
L1	10.1	133	14.9	103	28.3	96
L2	10.2	134	18.9	100	27.2	90
L4	12.0	105	19.2	103	28.8	98

Table 4: Values of $F_{n_d^*}^{stat}$ to generate n_d^* sub-laminates counted from the back face of the plate.

Laminate	Ply thickness h_p [mm]	Number of interfaces n	F_d [kN]	$F_{n_d^*}^{stat}$ [kN]
L1	0.181	30	9.94	$n_d^* = 10,$ 10.26
L2	0.363	14	7.60	$n_d^* = 7,$ 6.88
L4	0.725	6	5.50	$n_d^* = 4,$ 5.65